Ruthenium(II)-polpyridyl Zirconium(IV) metal-organic frameworks as a new class of sensitized solar cells.

William A. Maza, Andrew J. Haring, Spencer R. Ahrenholtz, Charity C. Epley, Shaoyang Lin, Amanda J. Morris

Department of Chemistry, Virginia Polytechnic Institute and State University, Blacksburg, VA 24061, United States

Experimental Details.

X-ray powder diffraction patterns (PXRD) of powdered samples were obtained with a Rigaku Miniflex, whereas thin film samples on TiO_2-FTO samples were obtained with a Pan Analytical X'PERT Pro each equipped with a CuKα radiation source (λ = 1.5418 Å) with a 0.8 deg/min scan rate (0.02º step size). Scanning electron microscopy (SEM) images were collected with a Leo/Zeiss 1550 Schottky field-emission scanning electron microscope equipped with an in-lens detector. X-ray photoelectron spectra (XPS) were collected with a Perkin Elmer dual anode X-ray source operating with monochromatic Mg Kα radiation (hν = 1253.6 eV) at 13 kV and 250 W (pass energy of 17.9 eV, and 0.1 step size). The operating pressure of the sample chamber was below 1×10^{-7} Torr and the photoelectrons were detected using a hemispherical analyzer. Analysis was performed on C 1s (range: 280-300 eV, 48 sweeps), N 1s (range: 390-410 eV, 192 sweeps), O 1s (range: 525-545 eV, 192 sweeps), Ru 3d (range: 277-297 eV, 192 sweeps), Ti 2p (range: 451-476 eV, 192 sweeps), and Zr 3d (range: 174-194 eV, 192 sweeps). The spectra were calibrated according to the C 1s peak, which is known to occur at 284.6 eV.[1] Thermal gravimetric analysis, TGA, was obtained using a TA Instruments Q500 TGA with a platinum pan, and all samples were heated at a rate of 10 °C min⁻¹ under a nitrogen atmosphere.

Steady-state UV-visible-NIR absorption and diffuse reflectance spectra were obtained using a Cary 5000 UV-vis-NIR spectrometer. Steady-state emission measurements were obtained using a Cary Eclipse Fluorescence spectrometer. The MOF powders were mounted on a glass slide using minimal amount of vacuum grease. Powder and film samples were positioned for front face excitation geometry and excited at 440 nm, 450 nm, and 460 nm to identify and correct for bands arising from either Raman scattering. A band pass filter was used on the emission side (allowed transmission 550 nm – 1100 nm).

Emission lifetimes were obtained by the time correlated single photon counting technique[2, 3] using a QuantaMaster QM-200-45E (PTI) equipped with a LED light source (510 nm, FWHM ~ 20nm, PTI) and PM-20 TCSPC module SPC-130. Samples were placed diagonally in a quartz cuvette, sealed and purged with N_2 for one hour. The sample decays were collected by a front-face illumination geometry and the emission lifetime values obtained using the DecayFit (www.fluortools.com) software package[4] by a deconvolution/reconvolution process with the instrument response function (IRF). Additional scatter from the substrate/sample was accounted for in the deconvolution process.

Powder X-ray Diffraction.
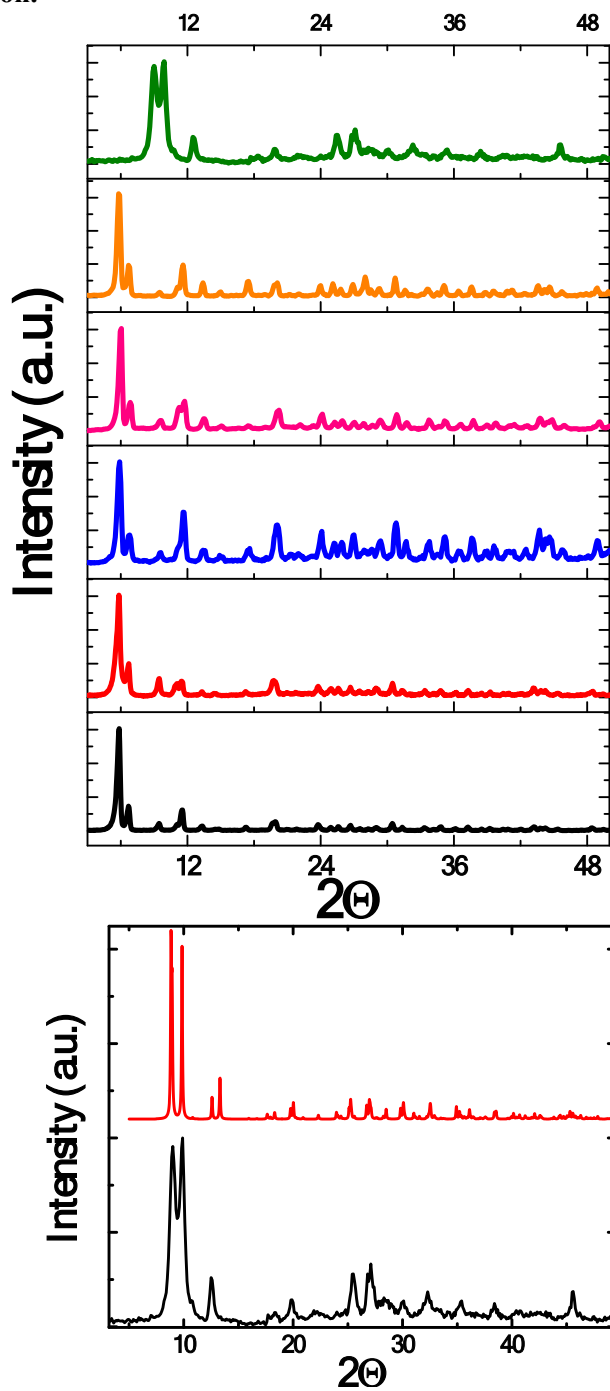
Figure S1a. (Top) Experimental X-ray powder diffraction patterns of UiO-67 (black), RuDCBPY-UiO-67 (red), UiO-67-DCBPY (blue), RuDCBPY-UiO-67-DCBPY-OP (pink), RuDCBPY-UiO-67-DCBPY-PS (orange), and RuDCBPY-ZrMOF (green). The PXRD pattern of the RuDCBPY-ZrMOF powder, though indicative of a highly crystalline material, was considerably different than that of UiO-67, UiO-67-DCBPY, RuDCBPY-UiO-67, and RuDCBPY-UiO-67-DCBPY. (Bottom) Comparison of the RuDCBPY-ZrMOF powder to the predicted PXRD pattern of ZrFA from reference[5].
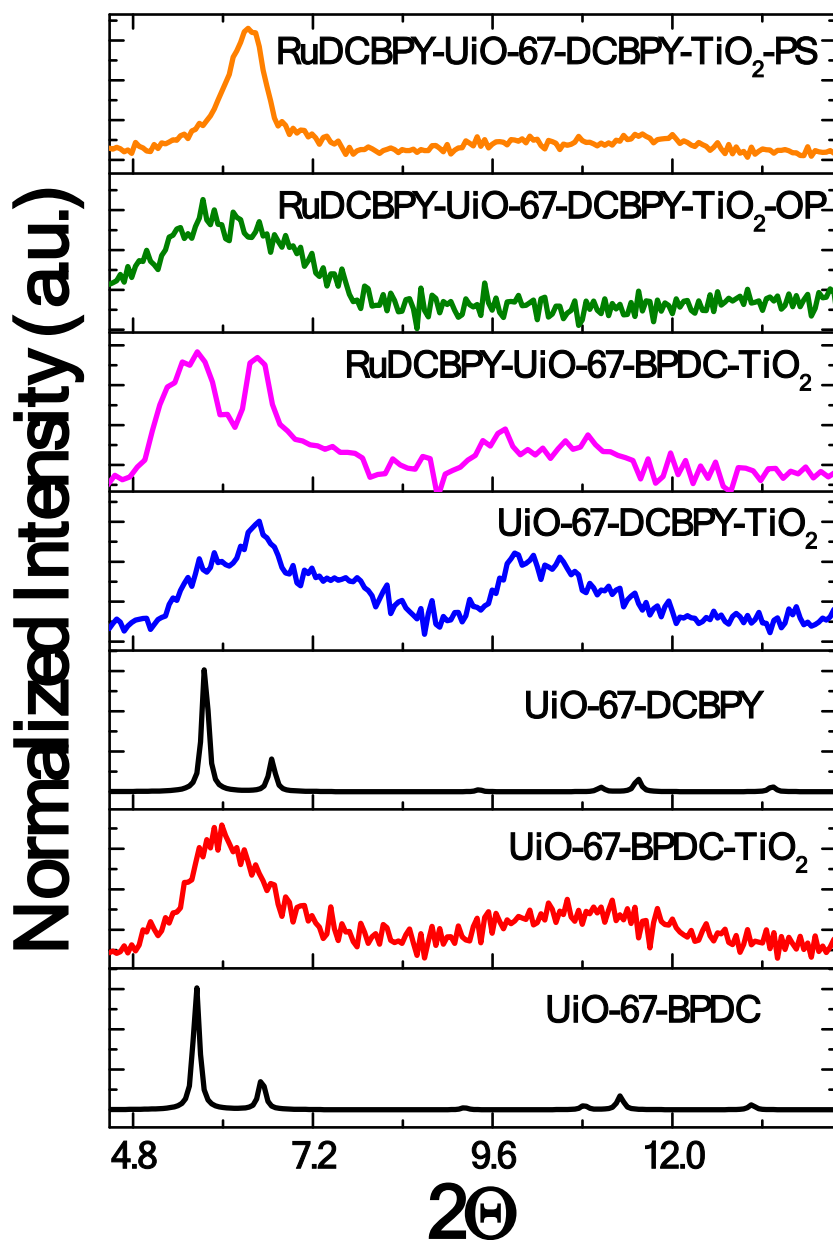
Figure S1b. Experimental low angle PXRD patterns of UiO-67-TiO$_2$ (red), UiO-67-DCBPY-DCBPY-TiO$_2$ (blue), RuDCBPY-UiO-67-TiO$_2$ (pink), RuDCBPY-UiO-67-DCBPY-OP-TiO$_2$ (green), and RuDCBPY-UiO-67-DCBPY-PS-TiO$_2$ (orange) compared to predicted patterns of UiO-67 and UiO-67-DCBPY simulated from crystallographic data. The poor diffraction quality of the films is likely due to the micron size of the MOF crystallites (see Figure S7c). However, the morphology of the UiO-67 variant MOF crystals are in good agreement with those shown in other reports.[6-8]
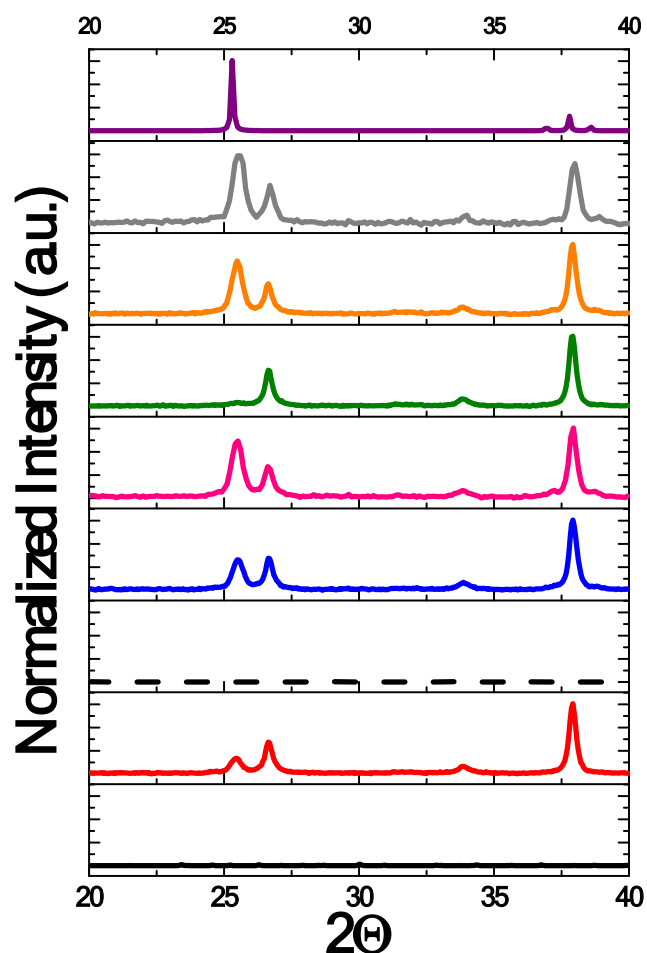
Figure S1c. Experimental high angle PXRD patterns of the UiO-67-TiO$_2$ (red), UiO-67-DCBPY-DCBPY-TiO$_2$ (blue), RuDCBPY-UiO-67-TiO$_2$ (pink), RuDCBPY-UiO-67-DCBPY-OP-TiO$_2$ (green), and RuDCBPY-UiO-67-DCBPY-PS-TiO$_2$ (orange) compared to experimental pattern of a TiO$_2$ layer on FTO (grey) and predicted patterns of anatase TiO$_2$ (purple), UiO-67 (black solid), and UiO-67-DCBPY (black dashed) simulated from crystallographic data.[9] The observed diffraction peaks correspond to the (101) plane of TiO$_2$ (2Θ ~ 25.6 °), the 110 plane of FTO (2Θ ~ 26.7 °), and overlapping signals at 38.1 ° corresponding to the FTO (211), and TiO$_2$ (103, 004, and 112) planes.[9, 10] (Note: The low and high angle diffraction were presented separately due to the large disparity in the observed intensities of the diffraction peaks between the low vs high angle signals.)

RuDCBPY-ZrMOF Characterization.

The PXRD pattern of the RuDCBPY-ZrMOF was compared to those of a number of Zr-based metal-organic frameworks and found that RuDCBPY-ZrMOF closely resembled the pattern pertaining to a two dimensional coordination polymer recently reported, ZrFA, comprised of Zr(IV) and formic acid (Figure S1).[5] This coordination polymer incorporates a $Zr_6O_4(OH)_4$ secondary building unit similar to the UiO-series of MOFs where the Zr(IV) metals of the ZrFA nodes are bridged by eight formic acid carboxylates. These $Zr_6O_4(OH)_4(COO^-)_8$ nodes are bridged by four additional formic acid carboxylate units to form the infinite two-dimensional sheets which non-covalently stack along the b-axis. Thermal gravimetric analysis of the RuDCBPY-ZrMOF also closely resembles that observed for ZrFA in that ZrFA displayed mass loss at approximately 50 °C, 201 °C, and 276 °C whereas RuDCBPY-ZrMOF presents mass loss at 43 °C, 209 °C, and 297 °C (Figure S2). It is likely, from these data, that the RuDCBPY-ZrMOF material is a RuDCBPY-doped version of ZrFA although the mode of interaction between RuDCBPY and the ZrFA framework is uncertain. It is clear, however, from the steady-state diffuse reflectance, steady-state emission, and emission lifetime decays that RuDCBPY is, at least, adsorbed into or onto the material.
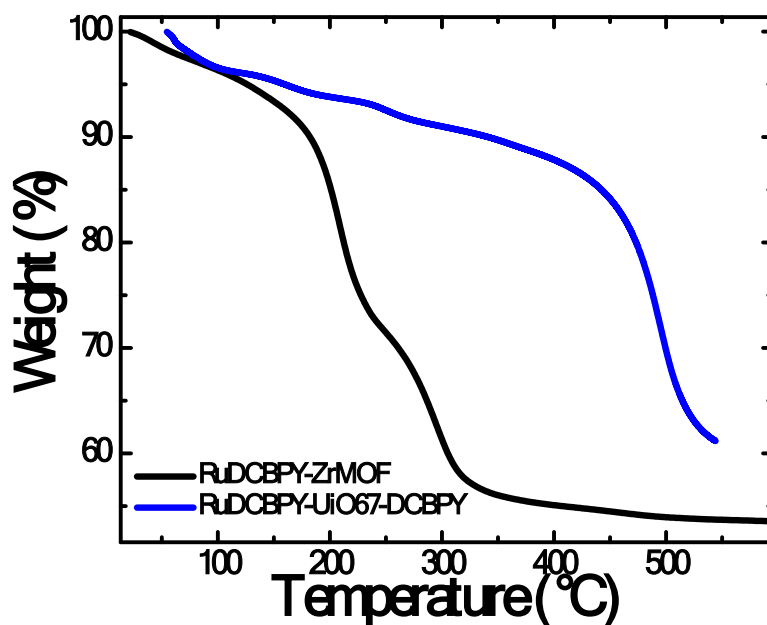
Figure S2. Thermogravimetric analysis of the RuDCBPY-ZrMOF powder (black) and RuDCBPY-UiO-67-DCBPY powder (blue). The ~10% loss of mass between 100 °C and 200 °C is attributed to loss of DMF solvent whereas the remaining losses between 200 °C – 250 °C and 250 °C – 300 °C are believed to be structural in nature corresponding to loss of the RuDCBPY ligand and global decomposition of the coordination polymer.[11]
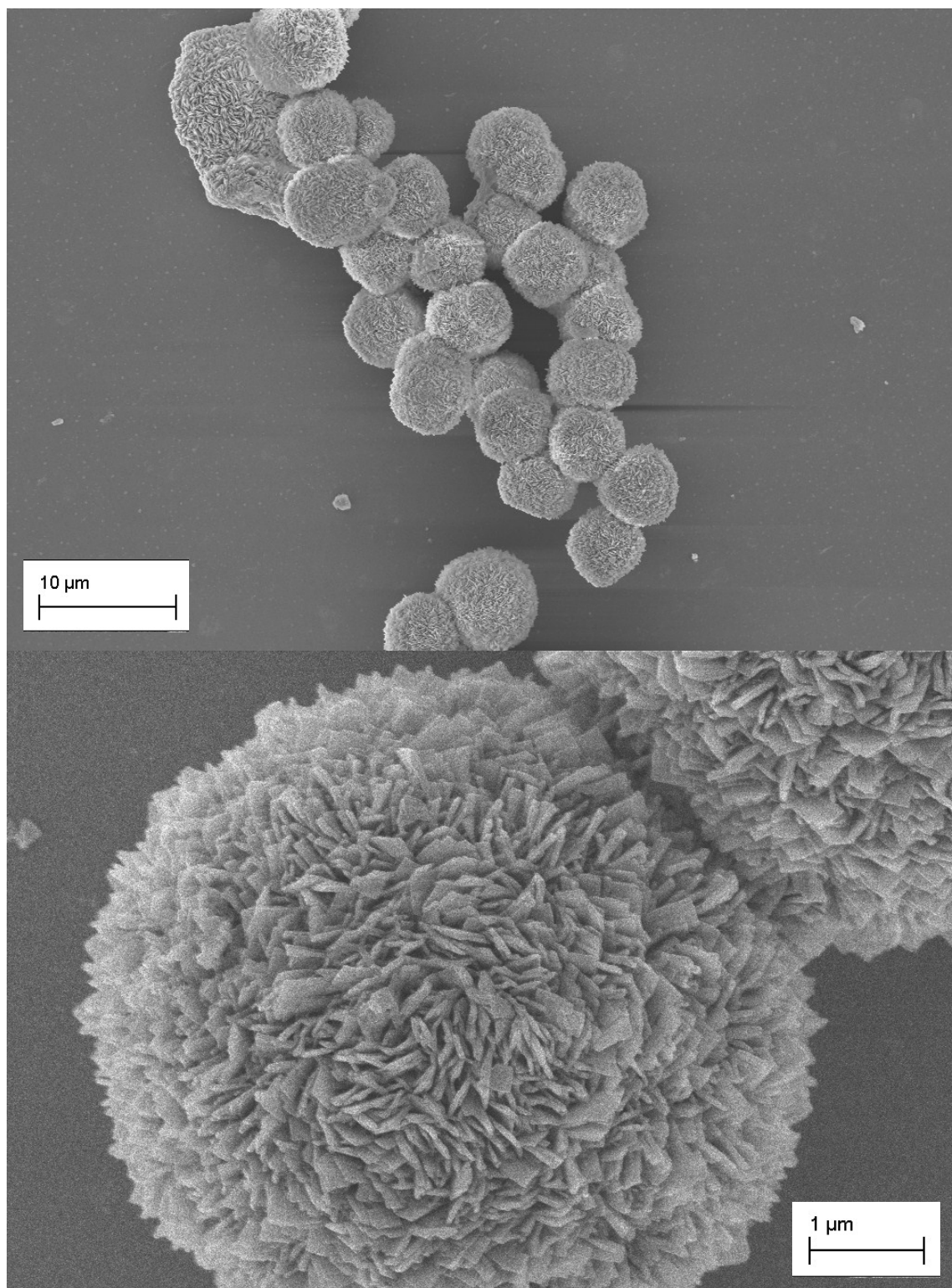
Figure S3. Scanning electron microscopy image of RuDCBPY-ZrMOF powder at 4,000 times (top), and 30,000 times (bottom) magnification.
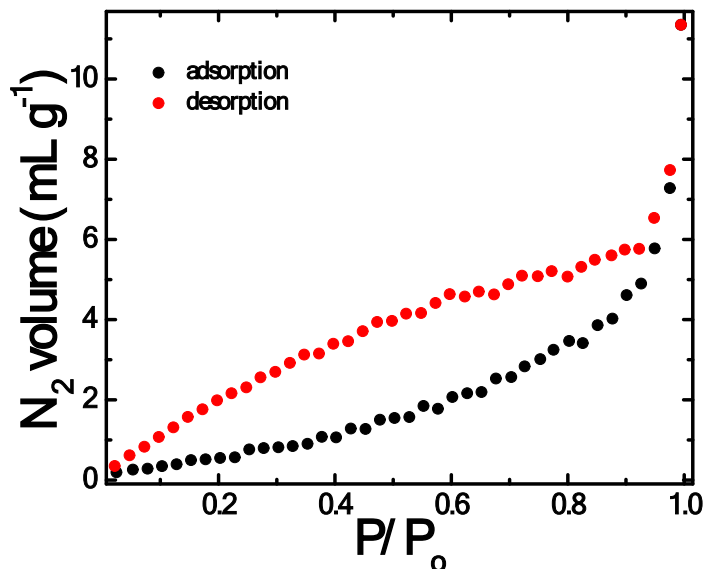
Figure S4. Nitrogen isotherm for RuDCBPY-ZrMOF powder. Nitrogen sorption-desorption isotherm measurements were obtained at 77 K using a Quantachrome Autosorb-1. A 0.09 g sample of RuDCBPY-ZrMOF degassed in a 6 mm large bulb sample cell was used for the measurements. Surface areas were obtained from fits of the isotherm data using the BET and Langmuir models.[12-14] BET and Langmuir surface area analysis indicate surface areas of 1.65 m^2/g and 149.5 m^2/g respectively.
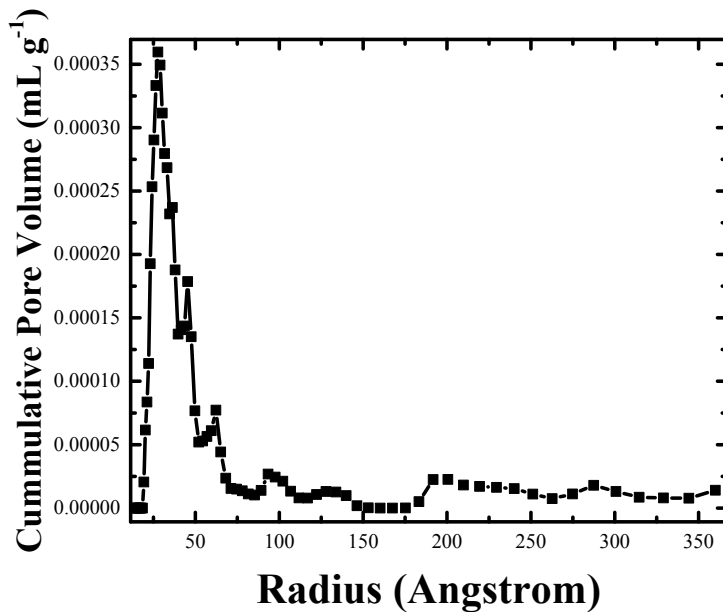
Figure S5. Calculated average pore volume of RuDCBPY-ZrMOF from isotherm data. The pore size distribution was calculated using a slit-pore equilibrium model by applying a non-local density functional theory method (NLDFT) to the raw data. All calculations were performed with the AS1Win v1.53 software package included with the Autosorb-1 instrument.
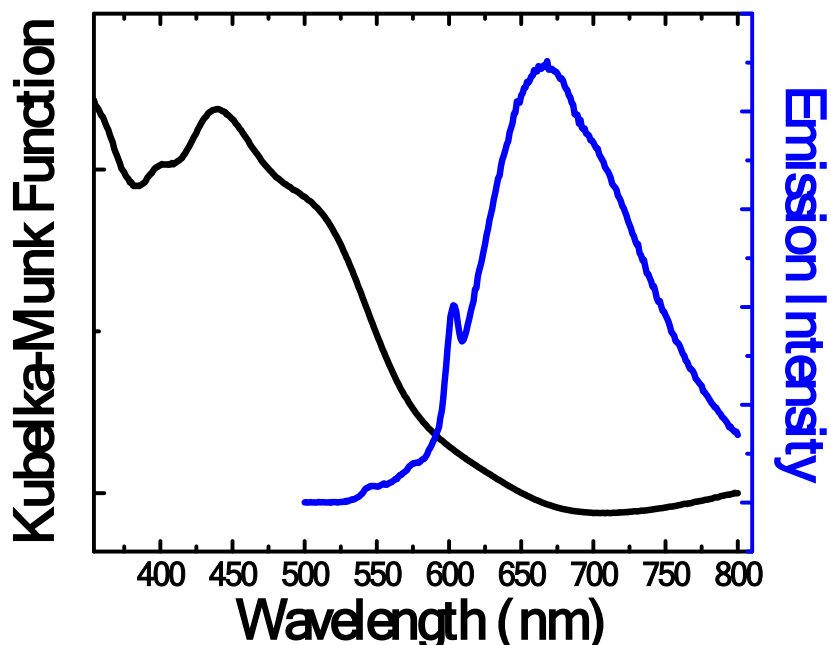
Figure S6. Steady-state diffuse reflectance (black) and emission (blue) spectra of RuDCBPY-ZrMOF powder (λ_{exc} = 440nm).

The spectral features of RuDCBPY-ZrMOF resemble that of RuDCBPY-UiO-67, RuDCBPY-UiO-67-DCBPY-OP, and RuDCBPY-UiO-67-DCBPY-PS (Figure S10 and S11). For example, the steady-state diffuse reflectance spectra displays an absorption maxima ~ 437 nm attributed to formation of the singlet metal-to-ligand charge transfer (^{1}MLCT) state of the RuDCBPY. The steady-state emission spectra presented an emission maxima around 645 nm is attributed to depopulation of the RuDCBPY ^{3}MLCT state. This was found to be somewhat red shifted relative to RuDCBPY in DMF solution (E_{3MLCT} ~625 nm) but very similar to the maxima observed for RuDCBPY-UiO-67 at higher doping concentrations (between 640 nm and 650 nm at doping concentrations above 20 m*m*).[6, 15, 16]

Scanning Electron Microscopy.
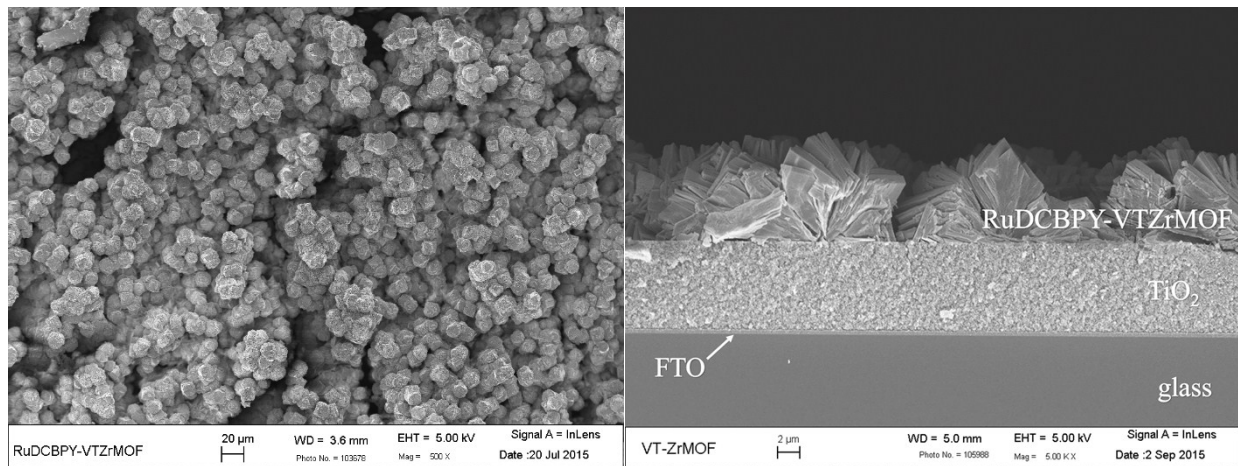
Figure S7a. Scanning electron microscopy images of a RuDCBPY-ZrMOF film grown on TiO_2 deposited on FTO; (left) view from the top, (right) side view.
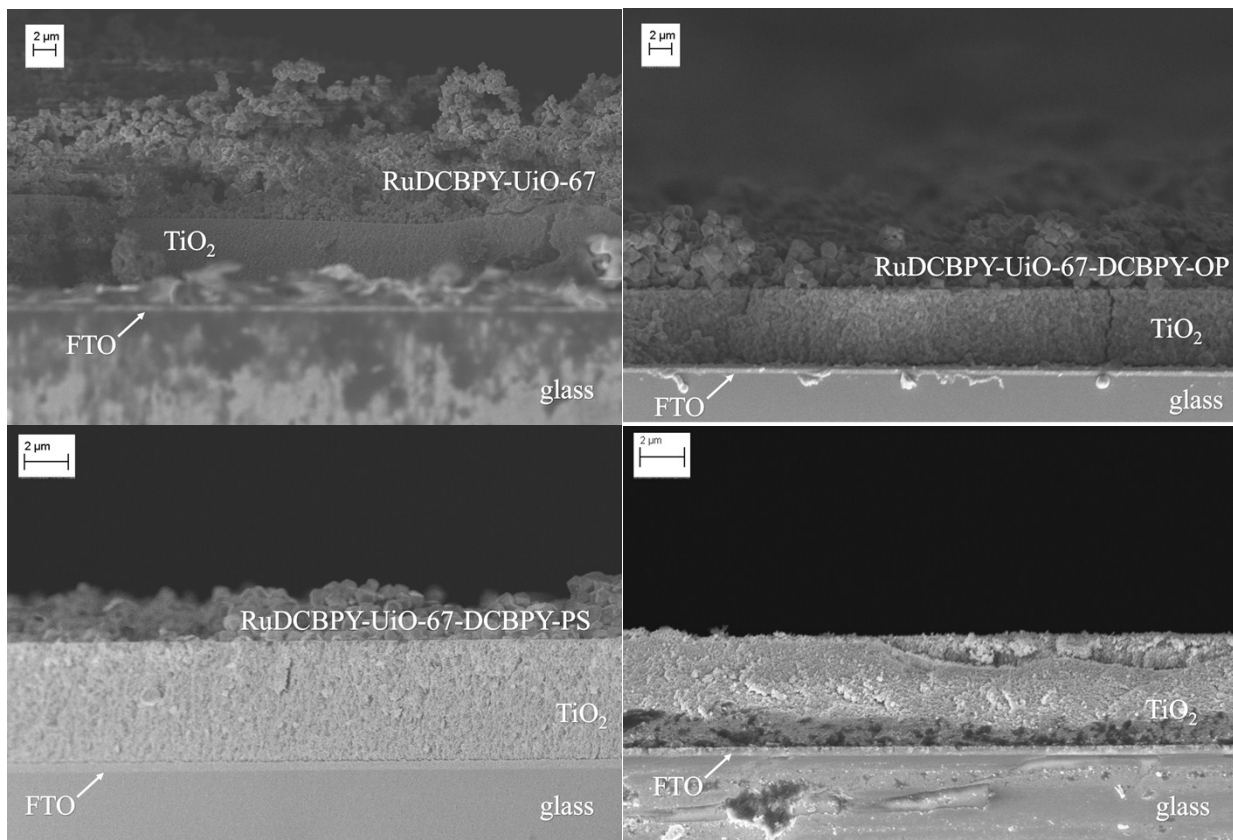
Figure S7b. Scanning electron microscopy side profile images of RuDCBPY-UiO-67 (top left), RuDCBPY-UiO-67-DCBPY-OP (top right), and RuDCBPY-UiO-67-DCBPY-PS (bottom left) films on TiO_2 compared to TiO2 on FTO (bottom right).
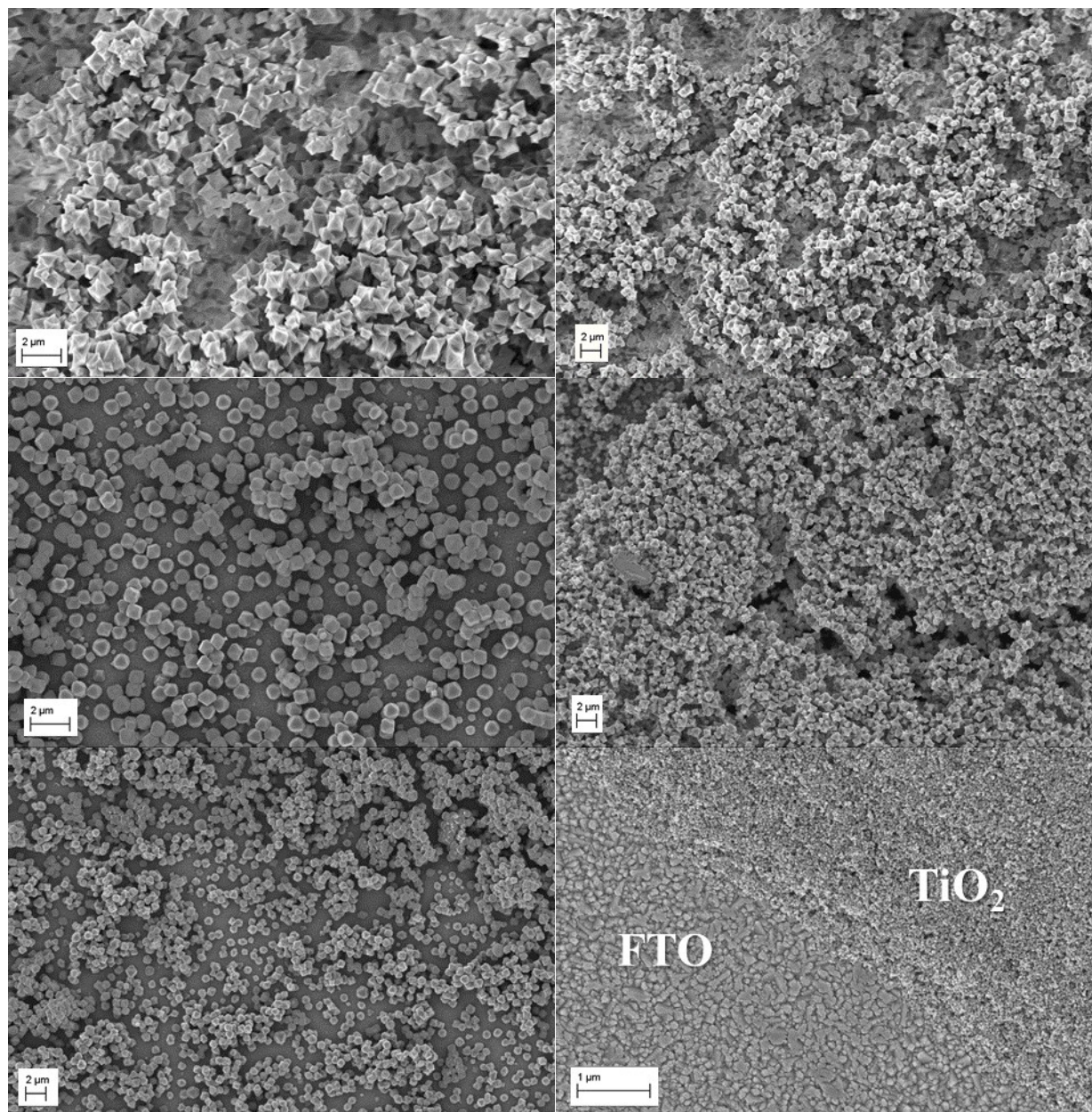
Figure S7c. Scanning electron microscopy top down images at 10,000 times magnification of RuDCBPY-UiO-67 (top left), RuDCBPY-UiO-67-DCBPY-OP (top right), and RuDCBPY-UiO-67-DCBPY-PS (middle left) films on TiO_2 compared to UiO-67 (middle right), UiO-67-DCBPY (bottom left) on TiO_2, and TiO_2 on FTO (bottom right). The crystallite morphology of the doped UiO-67 and UiO-67-DCBPY present as regular octahedra and truncated octahedra, respectively, and is consistent with what has been observed previously.[7, 8, 17]

Photophysical Characterization of Ru-MOF/TiO$_2$ Films.

RuDCBPY-UiO-67 powders and films have been characterized before.[6, 15] Negligible differences of the steady-state diffuse reflectance and emission spectra were observed for RuDCBPY-UiO-67 films grown onto TiO$_2$. These RuDCBPY-UiO-67-TiO$_2$ films display absorption maxima at ~ 430 nm with a small shoulder at approximately 475 nm. The steady-state emission spectra displays a maxima around 636 nm. Emission lifetime decays were best fit to a bi-exponential decay model corresponding to two populations of RuDCBPY within the MOF matrix: a fast ~ 35 ns component decay and a longer 388 ns component.

UiO-67-DCBPY films grown on TiO$_2$ were post-synthetically doped with RuDCBPY by diffusion of Ru(bpy)$_2$Cl$_2$ into the material with heat. The resulting films display an absorption maxima at 439 nm and an emission maxima at 640 nm. The emission lifetime decay of RuDCBPY-UiO-67-DCBPY-TiO$_2$ was best fit to a bi-exponential model yielding a fast component with a time constant of 13 ns and longer component with a time constant of 143 ns. Presumably, the UiO-67-DCBPY film is stable enough for the RuDCBPY to be prepared *in situ* without perturbation of the morphology of the material. Indeed, x-ray powder diffraction patterns (PXRD) of the post-synthetically modified powders support this assumption.

The emission lifetime decay of RuDCBPY-ZrMOF on TiO$_2$ was adequately fit to a bi-exponential function with a fast component of 2 ns and longer component of 204 ns. The fast component lifetime is considerably quenched relative to that lifetime observed for RuDCBPY-ZrMOF (16 ns) and RuDCBPY-UiO-67 (20 ns at 27 m*m* doping concentration) grown on FTO in the absence of TiO$_2$ suggesting a relatively strong interaction between RuDCBPY-ZrMOF and the TiO$_2$. The magnitude of the long lifetime component is reminiscent of the long lifetime component of RuDCBPY-doped UiO-67 films on FTO at higher doping concentrations (~150 ns at 27 m*m* doping concentration).[6]
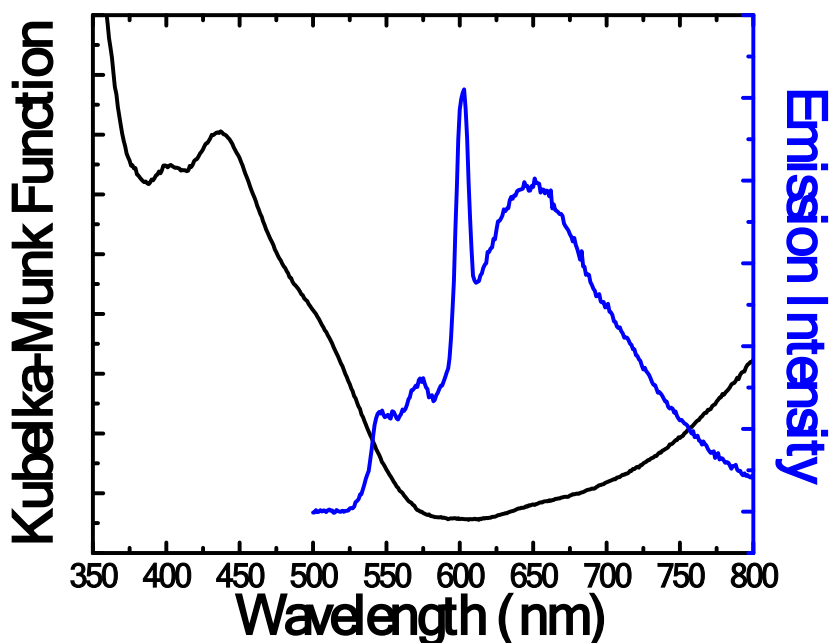
Figure S8. Steady-state diffuse reflectance (black) and emission spectra (blue) of RuDCBPY-ZrMOF thin film grown on TiO$_2$-FTO (λ_{exc} = 440nm).
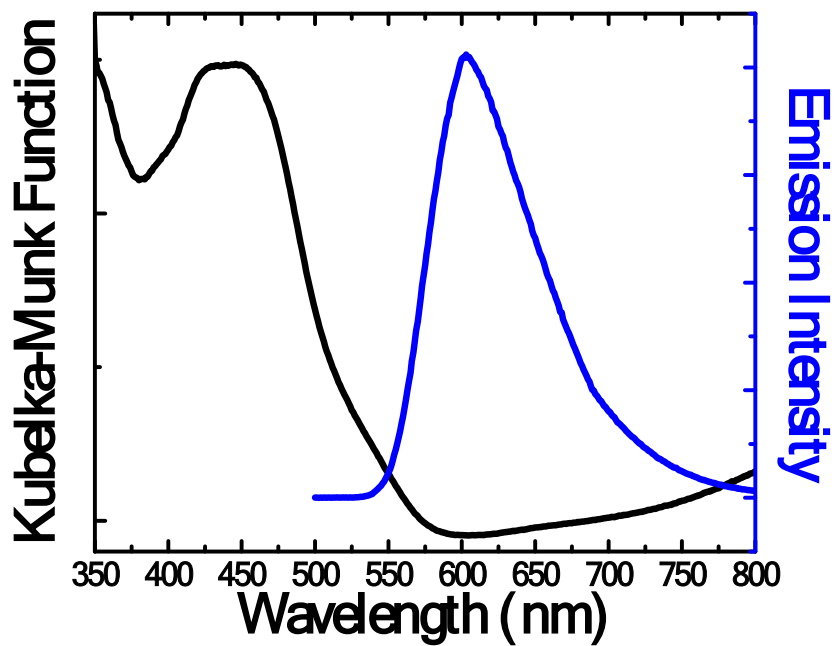
Figure S9. Steady-state diffuse reflectance (black) and emission (blue) spectra of RuBPY@UiO-67 thin film grown on TiO$_2$-FTO (λ_{exc} = 440nm).
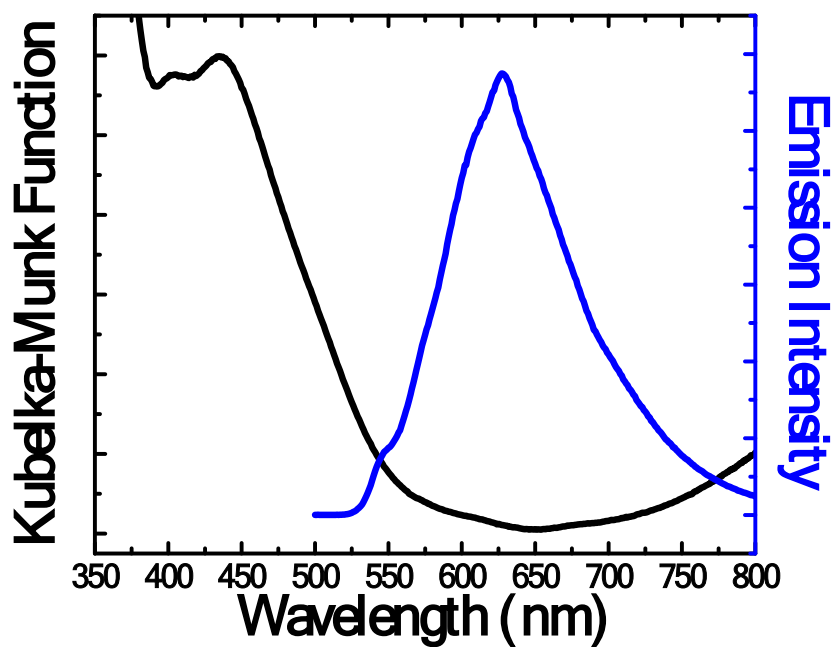
Figure S10. Steady-state diffuse reflectance (blue) and emission (blue) spectra of RuDCBPY-UiO-67-DCBPY-OP thin films grown on TiO$_2$-FTO (λ_{exc} = 440nm).
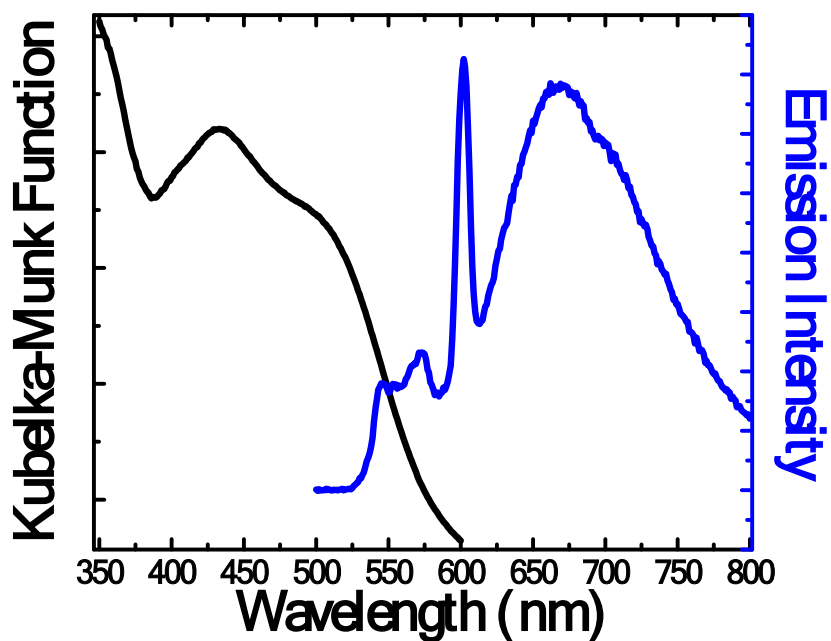
Figure S11. Steady-state diffuse reflectance (black) and emission (blue) spectra of RuDCBPY-UiO-67-DCBPY-PS grown on TiO2-FTO (λ_{exc} = 440nm).
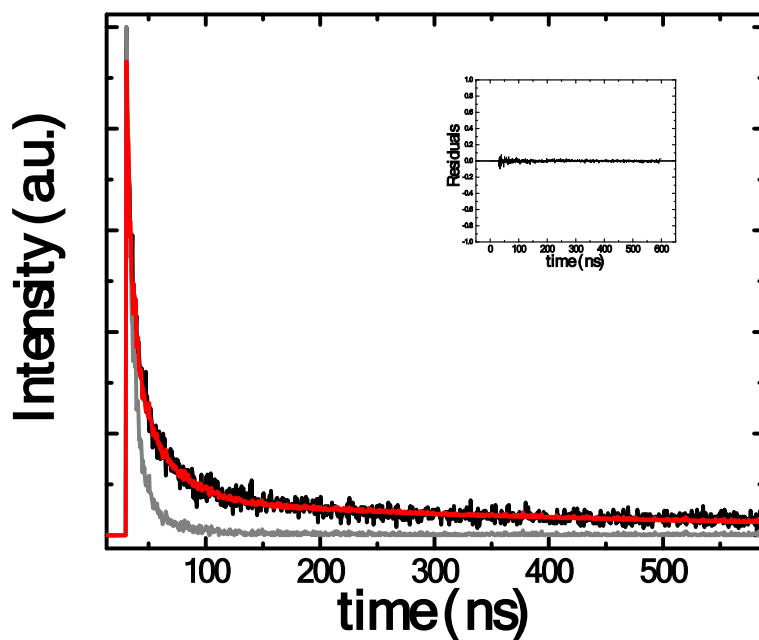
Figure S12. Emission lifetime decay (black) of a RuDCBPY adsorbed on TiO_2 and resulting fit (red) obtained using a deconvolution analysis. The inset shows the residuals obtained from the analysis. The instrument response function is shown in grey.
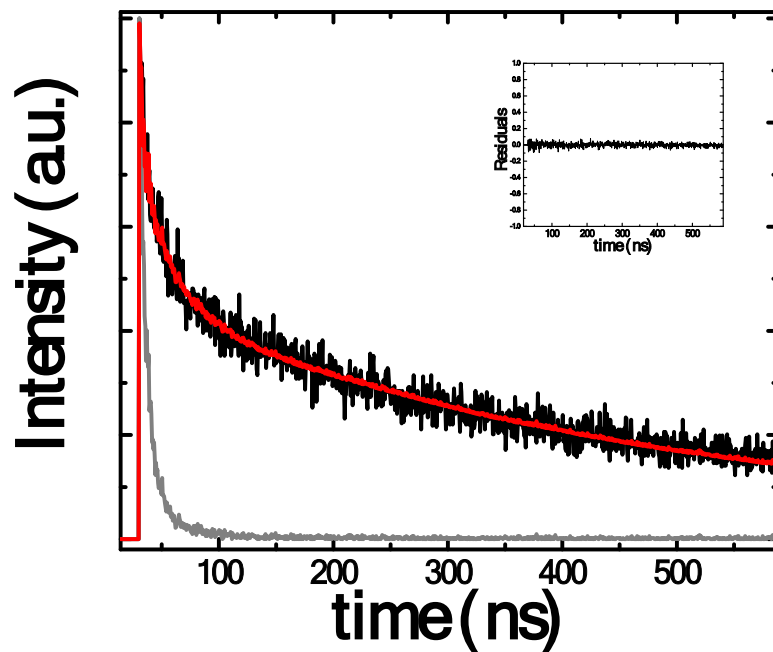
Figure S13. Emission lifetime decay (black) of a RuBPY@UiO-67 film grown on TiO$_2$ and resulting fit (red) obtained using a deconvolution analysis. The inset shows the residuals obtained from the analysis. The instrument response function is shown in grey.
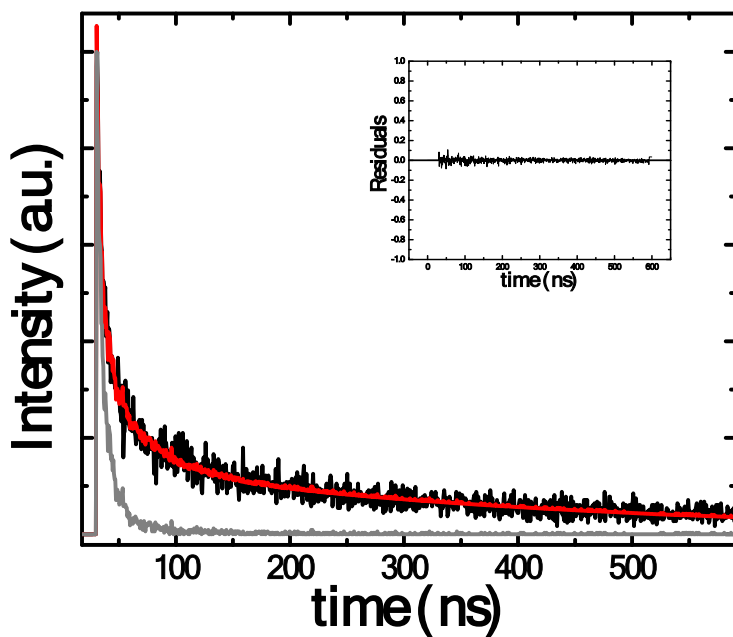
Figure S14. Emission lifetime decay (black) of a RuDCBPY-UiO-67 film grown on TiO$_2$ and resulting fit (red) obtained using a deconvolution analysis. The inset shows the residuals obtained from the analysis. The instrument response function is shown in grey.
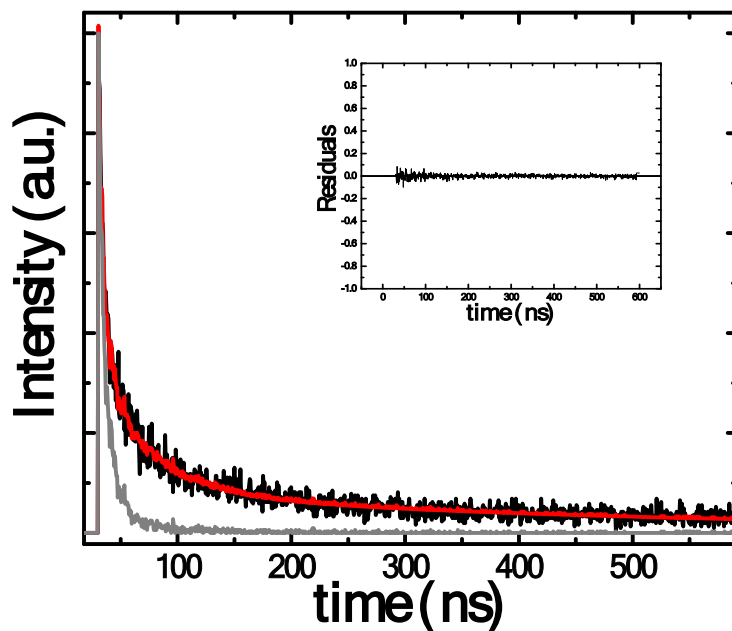
Figure S15. Emission lifetime decay (black) of a RuDCBPY-UiO-67 film grown on TiO$_2$ and resulting fit (red) obtained using a deconvolution analysis. The inset shows the residuals obtained from the analysis. The instrument response function is shown in grey.
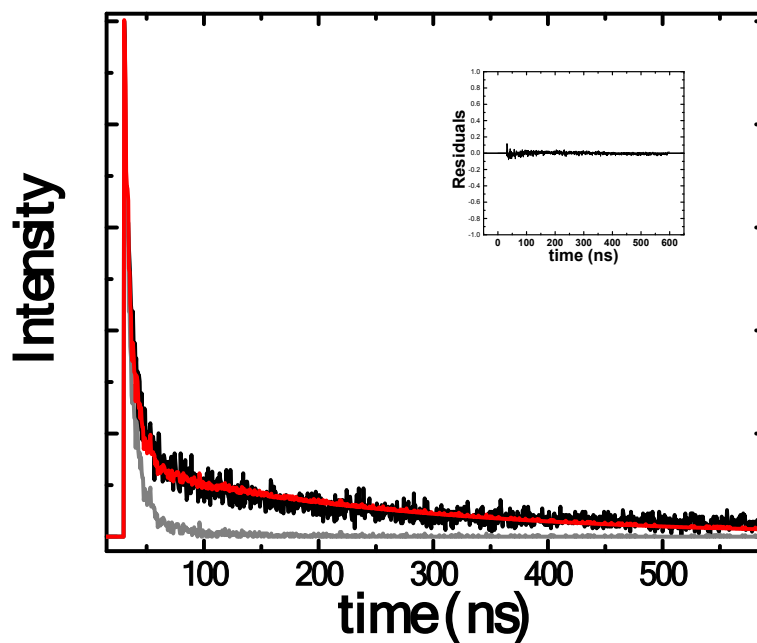
Figure S16. Emission lifetime decay (black) of a RuDCBPY-UiO-67-DCBPY film (prepared as one pot synthesis) grown on TiO$_2$ and resulting fit (red) obtained using a deconvolution analysis. The inset shows the residuals obtained from the analysis. The instrument response function is shown in grey.
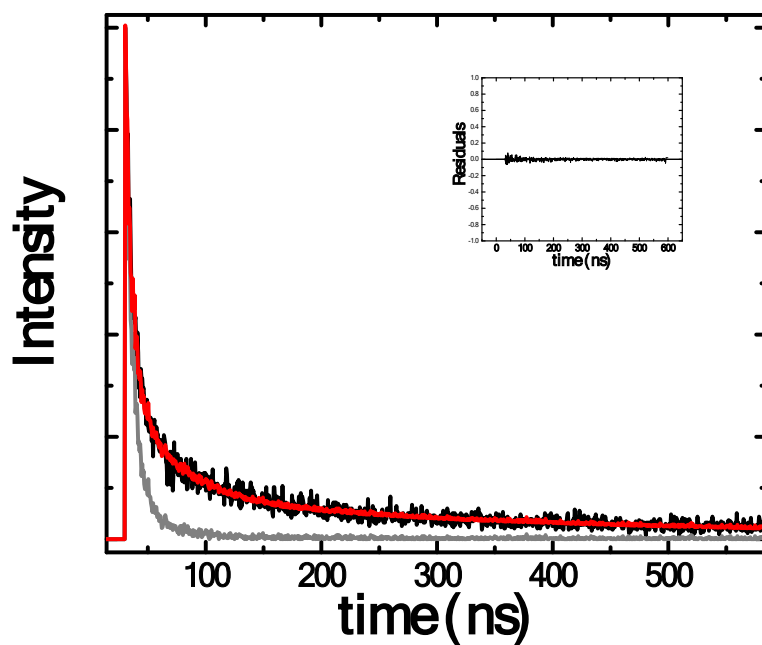
Figure S17. Emission lifetime decay (black) of a post synthetically doped RuDCBPY-UiO-67-DCBPY film grown on TiO$_2$ and resulting fit (red) obtained using a deconvolution analysis. The inset shows the residuals obtained from the analysis. The instrument response function is shown in grey.
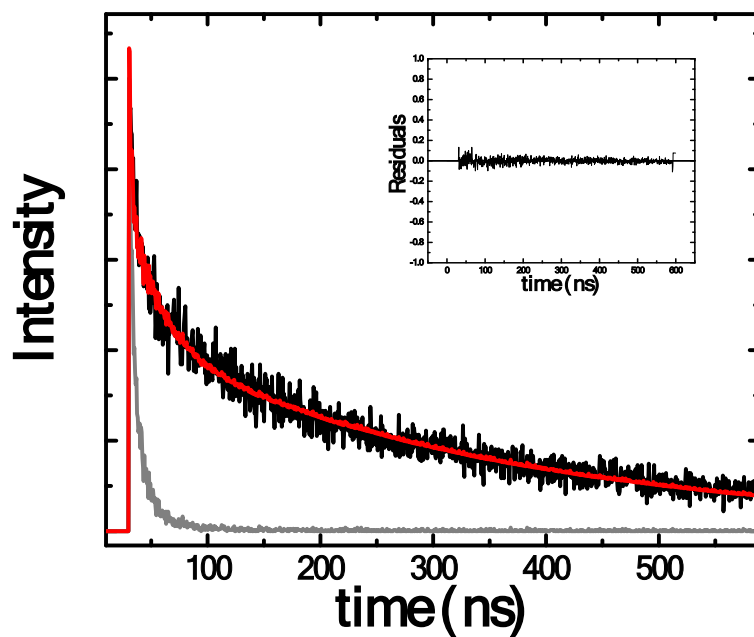
Figure S18. Emission lifetime decay (black) of a RuDCBPY-ZrMOF powder and resulting fit (red) obtained using a deconvolution analysis. The inset shows the residuals obtained from the analysis. The instrument response function is shown in grey.
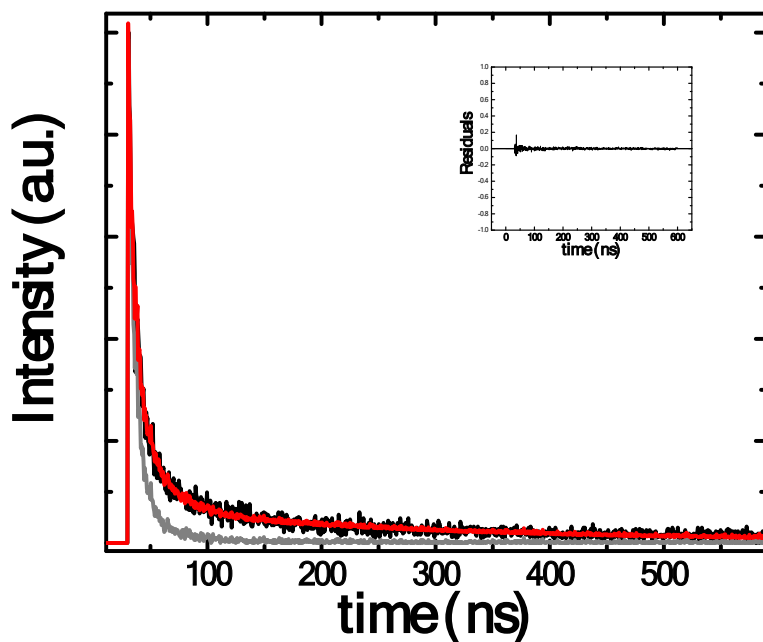
Figure S19. Emission lifetime decay (black) of a RuDCBPY-ZrMOF film grown on TiO_2 and resulting fit (red) obtained using a deconvolution analysis. The inset shows the residuals obtained from the analysis. The instrument response function is shown in grey.
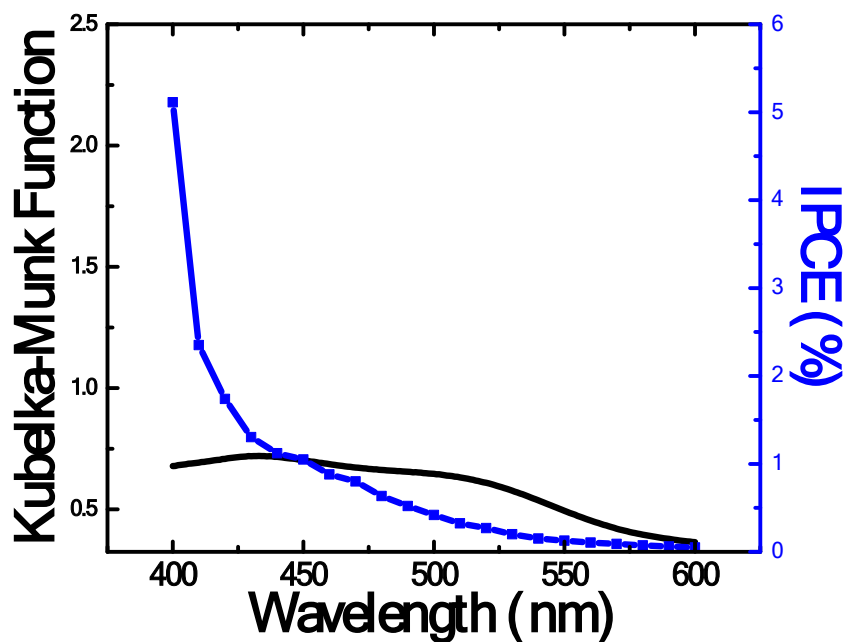
Figure S20. Overlay of the diffuse reflectance spectra (black) and IPCE spectra of RuDCBPY-UiO-67-DCBPY-TiO_2-PS.

References

1. J. F. Moulder and J. Chastain, *Handbook of X-ray Photoelectron Spectroscopy: A Reference Book of Standard Spectra for Identification and Interpretation of XPS Data*, Physical Electronics, 1995.
2. B. Valeur and M. N. Berberan-Santos, WileyVCH Weinheim, 2nd edn., 2012.
3. D. O'Connor, *Time-correlated single photon counting*, Academic Press, 1984.
4. F. DecayFit - Fluorescence Decay Analysis Software 1.3, www.fluortools.com.
5. W. B. Liang, R. Babarao, M. J. Murphy and D. M. D'Alessandro, *Dalton Trans.*, 2015, 44, 1516-1519.
6. W. A. Maza, S. R. Ahrenholtz, C. C. Epley, C. S. Day and A. J. Morris, *J. Phys. Chem. C.*, 2014, 118, 14200-14210.
7. H. H. Fei and S. M. Cohen, *Chem Commun.* 2014, 50, 4810-4812.
8. W. A. P. Maza, R.; Morris, A. J., *J. Am. Chem. Soc.*, 2015, 137, 8161-8168.
9. C. J. Howard, T. M. Sabine and F. Dickson, *Acta Crystallogr B.* 1991, 47, 462-468.
10. N. Chantarat, Y. W. Chen, S. H. Hsu, C. C. Lin, M. C. Chiang and S. Y. Chen, *Ecs J Solid State Sc.* 2013, 2, Q131-Q135.
11. M. M. Cooke, E. H. Doeven, C. F. Hogan, J. L. Adcock, G. P. McDermott, X. A. Conlan, N. W. Barnett, F. M. Pfeffer and P. S. Francis, *Anal. Chim. Acta.* 2009, 635, 94-101.
12. S. Brunauer, P. H. Emmett and E. Teller, *J. Am. Chem. Soc.*, 1938, 60, 309-319.
13. I. Langmuir, *J. Am. Chem. Soc.*, 1932, 54, 2798-2832.
14. S. Lowell, Shields, J.E., Thomas, M.A., Thommes, M., *Characterization of Porous Solids and Powders: Surface Area, Pore Size and Density*, Kluwer Academic, 2004.
15. W. A. Maza and A. J. Morris, *J. Phys. Chem. C.*, 2014, 118, 8803-8817.
16. P. H. Xie, Y. J. Hou, B. W. Zhang, Y. Cao, F. Wu, W. J. Tian and J. C. Shen, *J Chem Soc Dalton.* 1999, 4217-4221.
17. A. Schaate, P. Roy, A. Godt, J. Lippke, F. Waltz, M. Wiebcke and P. Behrens, *Chem-Eur J.* 2011, 17, 6643-6651.